Biophysical Journal Volume 108 February 2015 724–737

Article

Critical Examination of the Colloidal Particle Model of Globular Proteins

Prasad S. Sarangapani,[1] Steven D. Hudson,[2] Ronald L. Jones,[2] Jack F. Douglas,[2] and Jai A. Pathak[1,*]
[1]Formulation Sciences Department, MedImmune, Gaithersburg, Maryland; and [2]Materials Science and Engineering Division, National Institute of Standards and Technology, Gaithersburg, Maryland

ABSTRACT Recent studies of globular protein solutions have uniformly adopted a colloidal view of proteins as particles, a perspective that neglects the polymeric primary structure of these biological macromolecules, their intrinsic flexibility, and their ability to sample a large configurational space. While the colloidal perspective often serves as a useful idealization in many cases, the macromolecular identity of proteins must reveal itself under thermodynamic conditions in which the native state is no longer stable, such as denaturing solvents and high protein concentrations where macromolecules tend to have screened excluded volume, charge, and hydrodynamic interactions. Under extreme pH conditions, charge repulsion interactions within the protein chain can overcome the attractive hydrogen-bonding interactions, holding it in its native globular state. Conformational changes can therefore be expected to have great significance on the shear viscosity and other rheological properties of protein solutions. These changes are not envisioned in conventional colloidal protein models and we have initiated an investigation of the scattering and rheological properties of model proteins. We initiate this effort by considering bovine serum albumin because it is a globular protein whose solution properties have also been extensively investigated as a function of pH, temperature, ionic strength, and concentration. As we anticipated, near-ultraviolet circular dichroism measurements and intrinsic viscosity measurements clearly indicate that the bovine serum albumin tertiary structure changes as protein concentration and pH are varied. Our findings point to limited validity of the colloidal protein model and to the need for further consideration and quantification of the effects of conformational changes on protein solution viscosity, protein association, and the phase behavior. Small-angle Neutron Scattering measurements have allowed us to assess how these conformational changes influence protein size, shape, and interprotein interaction strength.

INTRODUCTION

Proteins are polyampholytes, a type of charged polymer containing both acidic and basic functional groups, with pH- and concentration-dependent conformations (1–4). As with synthetic polymers, these macromolecules may adopt collapsed or highly extended configurational states and exhibit a wide range of conformations, even in their biologically active and relatively compact globular form. When denaturants are added to protein solutions, globular proteins transform configurationally into open polymer structures exhibiting a conformational structure remarkably similar to synthetic polymers in good solvents and can be modeled reasonably as self-avoiding walks (5,6). Recent modeling of protein solutions has heavily emphasized a coarse-grained model of globular proteins as being rigid sphere-like or perhaps ellipsoidal colloidal particles as a matter of mathematical expediency (7–9). Although this type of idealization has clearly been useful for many purposes, as in the case of flexible polymers in solution, the colloidal model clearly has its limitations, and we must know the conditions when this type of modeling is untenable.

Of course, there are good reasons to expect that varying pH over a large range, the addition of denaturant additives, the adsorption of proteins onto surfaces, and strong shear should denature proteins, i.e., convert them into another globule state or to a nonglobular state, thereby making these molecules prone to supramolecular aggregation. Because synthetic polymers normally exhibit screening of their excluded volume interactions with an increase in polymer concentration, we may also expect some unraveling of proteins and a loss of solution stability with increasing protein concentration, even under tightly controlled pH conditions (a phenomenon with large potential consequences for drug delivery because of the large viscosity increase that normally accompanies such aggregation processes (10,11)). To address these issues, we must modify the colloidal protein model to account for interactions deriving from changes in conformational structure with thermodynamic conditions or nonequilibrium driving conditions such as solution shear.

Perturbations to conformation can also have dramatic effects on intermolecular interactions and stability in the crowded environment of the cell and concentrated (>100 mg/mL) therapeutic protein formulations (12–19). The interrelationship among conformation, intermolecular interactions, and solution viscosity at high concentrations is

Submitted September 19, 2014, and accepted for publication November 5, 2014.

*Correspondence: pathakj@medimmune.com

Prasad S. Sarangapani's present address is Regeneron Pharmaceuticals, 777 Old Saw Mill River Rd, Tarrytown, NY 10591.

Editor: Nathan Baker.

0006-3495/15/02/0724/14 $2.00

http://dx.doi.org/10.1016/j.bpj.2014.11.3483

thus a problem of significant interest to the biophysics and biochemistry communities, as well as the biopharmaceutical industry. Protein conformational structure and stability to thermodynamic conditions are basic to the control and understanding of protein function (3,13,18–20).

Based on these general observations and considerations, we have initiated an experimental program with an aim to better characterize the conformational structure and stability, starting with well-studied proteins.

Because proteins possess a pH-dependent net charge and conformational structure, it is natural to begin our study with a consideration of how pH changes protein solution behavior (1,2,21–28). In particular, we focus our attention on bovine serum albumin (BSA), an extensively studied single domain globular protein with tunable pH-dependent conformations and solution viscosity (1,24,25,29–31). BSA is therefore a useful model system in this regard. The results of Fig. 1 clearly demonstrate that BSA solutions in water exhibit a complex pH dependence and concentration dependence, as expected from our general discussion above. BSA has been reported to undergo a series of concentration-dependent reversible conformational transitions for $c > 10$ mg/mL (1,30).

Prior studies of the pH dependence of dilute BSA solutions attributed the minimum in the viscosity of the type shown in Fig. 1 to the electroviscous effect (32), while the maximum in the viscosity of solutions in aqueous buffers above 100 mg/mL is normally attributed to a reversible self-association of the proteins into a dynamic network at such high protein concentrations (25,32). The composition gradient multiangle light-scattering data on 40 mg/mL BSA solutions shown in Fig. S1 of the Supporting Material suggest that reversible self-association occurs over the entire pH range investigated and consists of monomer-dimer-octamer equilibrium in solution. Therefore, the interpretation of a viscosity maximum in terms of aggregation is not really justifiable. We know that polymer phase behavior and stability is normally affected by shape-dependent and orientationally dependent interactions, and proteins are not exceptional polymers in this regard (33,34).

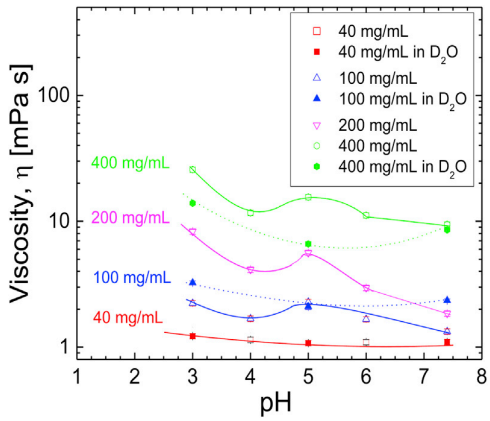

FIGURE 1 Infinite shear viscosity (measured at $\dot{\gamma} = 3 \times 10^4$ s^{-1}) for BSA solutions across the concentration (c) range 40 mg/mL $\leq c \leq$ 400 mg/mL and pH range 3.0 $\leq$ pH $\leq$ 7.4 in H_2O (*open symbols*) and D_2O (*solid symbols*) for pH values 3.0, 5.0, and 7.4. Lines that connect points merely aid visualization. Each data point is the average of five independent measurements, and in many cases, uncertainty estimates are smaller than the symbol size.

For completeness, we report pH-dependent high-shear viscosity of BSA in buffered D_2O solutions because our small-angle neutron scattering (SANS) measurements requires buffered D_2O solutions for scattering contrast purposes. Interestingly, we see that the solution behavior of BSA is significantly altered in D_2O, where a clear minimum in the viscosity is observed at the pI, even at 400 mg/mL. Hence, the electroviscous effect, which predicts a minimum in viscosity at the pI, applies differently in D_2O versus H_2O. Whereas in H_2O a viscosity minimum occurs only in dilute solutions, in D_2O it occurs in the dilute limit and applies to concentrated solutions as well.

Other investigators (7,29,35–43,45) of BSA have tended to model globular proteins as rigid monodisperse ellipsoidal or spherical particles (7–9,24,30,35,37,40,43–56). Although proteins have commonalities with colloid particles, and a colloidal view of protein solution thermodynamics is mathematically expedient (57–61), a purely colloidal view of proteins ignores their macromolecular identity (3,14,24,31,62,63), the focus of this work. In our treatment of our SANS measurements, we do our best to avoid assumptions regarding protein molecular shape and size polydispersity, although this type of analysis could be improved by having an even more molecularly faithful description of protein conformational structure than our modeling tools allow.

Standard biophysical assays such as dynamic light scattering (DLS) and size-exclusion chromatography are limited in their capability in providing simultaneous information regarding conformation and intermolecular interactions in protein solutions (64–70). Thus, we also employ near-UV circular dichroism (CD) and SANS together to understand how molecular conformation and intermolecular interactions influence solution rheology data, because pH and BSA concentrations are varied. The collective analysis of our data indicates that varying protein concentration and pH leads to clear evidence for conformational changes in the BSA molecules, as quantified through the static structure factor of the protein solution, and solution rheology (Fig. 2).

MATERIALS AND METHODS

Lyophilized BSA powder (A7906, >99.7% protein, essentially fatty-acid free; Sigma-Aldrich, St. Louis, MO) of molar mass $M_w = 67$ KDa was dissolved at 20 mM ionic strength (I) in buffers in D_2O (99.9% D; Sigma-Aldrich) and H_2O (HPLC grade; J. T. Baker, Avantor, Center Valley, PA), respectively. The purity of all buffer salts and acids is 100%. These buffers comprised sodium citrate/citric acid at pH 3.0, sodium acetate/acetic acid at pH values 4.0 and 5.0, histidine hydrochloride at pH 6.0, and phosphate-buffered saline at pH 7.4. Stock solutions were prepared at 500 mg/mL

BSA concentration by dissolving the appropriate mass of lyophilized BSA in 100 mL of buffered D_2O or H_2O solutions that were prefiltered with 0.02 μm Anotop 10 syringe filter (Lot No. D140746; Whatman, GE Healthcare, Piscataway, NJ). Complete dissolution of the powder in appropriate buffers occurred quiescently between 2°C and 8°C for up to 72 h. The solutions were subsequently filtered through 0.22 μm filters of poly(ethersulfone) membranes (Lot No. 1085211; Thermo Scientific, Billerica, MA) and were gravimetrically diluted to the final BSA concentration, which was measured using absorbance at λ (wavelength) = 280 nm (A_{280}) on a model No. 8453 UV-visible spectrophotometer (Agilent Technologies, Santa Clara, CA). An absorbance coefficient of $\varepsilon_{280} = 0.667$ cm^2/mg (24) was used for BSA. All solutions were stored between 2°C and 8°C until use. Although other proteins (71) have shown a greater propensity for aggregation in the presence of D_2O, we found no evidence of aggregation of BSA solutions over the course of several months using DLS.

DLS was used to measure mutual diffusion coefficients, D_m, of BSA solutions between $c = 2$ mg/mL and 12 mg/mL on a DynaPro plate reader (Wyatt Technology, Santa Barbara, CA) with a light scattering detector sensitive to a wavelength $\lambda = 833$ nm and at fixed scattering angle (θ)= 130°. A linear fit of D_m versus concentration, c, is $D_m = D_o(1+k_Dc)$ (72,73), where D_o denotes the self-diffusion coefficient. Plots of D_m/D_o were used to characterize conformational changes in solution.

Near-UV CD measurements were performed in triplicate on each sample using a model No. J-815 spectropolarimeter (JASCO, Easton, MD) equipped with a 150 W Xenon arc lamp. Measurements were acquired with a bandwidth of 1 nm and a scan speed of 20 nm/min across a wavelength (λ) range 250 nm $\leq \lambda \leq$ 350 nm. Calibration was performed using a standard (+)-10-camphorsulfonic acid solution. A quantity of 1-mm path-length cuvettes (cat. no. 20-Q-1; Starna, Atascadero, CA), were used for dilute ($c \leq 10$ mg/mL) samples and 0.1 mm path-length cuvettes (cat. no. 20-C/Q-0.1; Starna) for higher concentration ($c = 100$ mg/mL) measurements. The path length was accepted on vendor specifications, and not verified. The high tension voltage remained <200 V for measurements at high concentrations, indicating that the absorbance was small enough to not adversely affect data quality. Cuvettes were carefully cleaned after each measurement by repeated rinsing using a concentrated cleaning solution provided by the vendor (Starna) and deionized water. All data were normalized by concentration and number of residues to be reported as molar ellipticity, $\theta = 100 \times \theta_\lambda/m \times d$, where θ_λ is the observed ellipticity at λ, and d and m denote path length and molar concentration, respectively.

SANS was performed on the NG-B beamline at the National Institute of Standards and Technology (NIST) Center for Neutron Research with neutron $\lambda = 0.5$ nm and $\lambda = 1.6$ nm ($\Delta\lambda$ / $\lambda = 0.15$), respectively, and sample-detector distances of 1.1 m and 5 m. These configurations lead to wave-vector, q, in the range 0.034 nm$^{-1} < q < 6.8$ nm^{-1}, where $q = (4\pi/\lambda)\sin(\Theta/2)$ and Θ denotes the scattering angle. Data reduction and analysis were subsequently performed in the software IGOR PRO Ver. 6.2 (WaveMetrics, Portland, OR) using algorithms (74) developed at the NIST Center for Neutron Research that correct for background electric noise, empty cell scattering, and buffer scattering. The procedure described in Kline (74) was followed without any modifications. Model fits to the scattering data were performed using nonlinear regression in IGOR PRO, which provided an average and uncertainty estimates of fit parameters. Details of the statistical mechanical model are described in the Supporting Material.

Rheology of aqueous solutions and solutions in deuterium oxide was measured over a shear rate ($\dot{\gamma}$) range of 3×10^4 s$^{-1} \leq \dot{\gamma} \leq 1.2 \times 10^5$ s^{-1} using a micro-slit m-VROC rheometer (Rheosense, San Ramon, CA) equipped with a Type-D chip. The Type-D chip senses a maximum pressure drop, ΔP, up to 800 KPa and has a minimum resolution of 1.2 KPa. This range of shear rate, although narrow, allows us to compare our results to a prior study of the pH dependence of BSA solution rheology at 10^7 s^{-1} (27), because BSA solutions respond in the infinite shear (second Newtonian) plateau at these shear rates.

Colloidal model for protein-protein interactions

The scattering intensity, $I(q)$, for a one-component monodisperse system can be written formally as

$$I(q) = \varphi V \Delta\rho^2 P(q) S(q) + B, \tag{1}$$

where φ is the volume fraction, V is the volume of a protein monomer, $\Delta\rho$ is the difference in scattering length density between the protein and the solvent ($\approx 2.47 \times 10^{-4}$ nm^{-2}), $P(q)$ is the form factor, $S(q)$ is the structure factor, and B is the background (75). The term $P(q)$ will be discussed in Results and Discussion and the Supporting Material in detail. We define φ for BSA as in previous work (24), while considering that SANS is a scattering static technique:

$$\varphi = \frac{m_{\mathrm{BSA}}\overline{\nu}_{\mathrm{BSA}}}{V_w + m_{\mathrm{BSA}}\overline{\nu}_{\mathrm{BSA}}}. \tag{2}$$

Here, V_w and m_{BSA} denote solvent (water) volume and BSA mass, respectively, while $\overline{\nu}_{\mathrm{BSA}}$ denotes the partial specific volume of BSA (21). We assume that $\overline{\nu}_{\mathrm{BSA}}$ is unaffected by isotopic substitution.

For fitting the scattering data, we introduce a random phase approximation (RPA) model of the protein based on a particle model with attractive and repulsive contributions, while accounting for site-specific short-ranged patchy interactions that are ubiquitous in protein solutions. This is clearly a coarse-grained model of the protein in the spirit of former colloidal models and our preference would be to avoid such models completely. Nonetheless, we feel this type of model is useful for characterizing the qualitative nature of the interprotein interaction strength. We develop this type of model to account for polymeric aspects (e.g., molecular size and shape, interprotein interaction strength) that naturally derive from the protein conformational changes evidenced by our independent spectroscopic observations on protein solutions under the same thermodynamic conditions of the protein as best we can.

Because the net charge of the proteins can be tuned by pH or additives, we use the RPA (76–80). The RPA has been applied to the analysis of x-ray scattering data on BSA by Barbosa et al. (1) and osmometry measurements on BSA with added salt by Wu and Prausnitz (81). Wu and Prausnitz (81) modeled osmotic contributions due to DLVO forces as a perturbation to the reference (hard-sphere) system. Using the RPA, we may then express $I(q)$ as

$$I(q) = \varphi V \Delta\rho^2 P(q)\left(S_0(q)[1 + \gamma U'(q) S_0(q)]^{-1}\right). \tag{3}$$

Here, $S_o(q)$, $U'(q)$, and γ are the reference structure factor, perturbation potential, and perturbation parameter, respectively, where $\gamma = 1$ over the investigated range. The scattering intensity in the thermodynamic limit $q \to 0$ can be related to the osmotic pressure of the system. Thus, osmotic pressure measurements can be related to small-angle scattering data via the following equation (82):

$$I(q \to 0) = (RT/M_w)(\partial\Pi/\partial c)^{-1}. \tag{4}$$

Here, the symbols Π, R, and T denote the osmotic pressure, ideal gas constant, and temperature ($T = 298$ K), respectively.

Our approach is well justified because we have previously shown (24) that the second osmotic virial coefficient (B_{22}) is negative at the pI, where intermolecular attractions dominate. Moreover, $B_{22} > 0$ is for pH distinct from the pI, which indicates net repulsive interactions, likely of Coulombic origin. Thus, intermolecular interactions can be tuned continuously across the pH range studied. However, to capture the short-range patchy interactions in protein solutions (83), a suitable reference system is required. We acknowledge that in the absence of any models directly derived for proteins, we are forced to approximate proteins as colloids to model patchy interactions using the Baxter sticky sphere (BSS) model. Indeed, colloidal approaches to protein solution hydrodynamics and thermodynamics have been applied to protein solutions as a mathematically expedient way to capture the physicochemical properties of proteins.

The highly coarse-grained approaches of Mehl et al. (40), Edsall (46), and Tanford et al. (30) used intrinsic viscosity data to describe the apparent shapes of proteins in solution. From these studies, a colloidal view of protein solutions became deeply entrenched in the literature (33,34,83). This colloidal approximation is inappropriate for modeling proteins due to the orientation dependence of protein-protein thermodynamic and hydrodynamic interactions. Wertheim's theory of associating fluids (84–87) can potentially capture dimerization and even multipolar interactions in associating fluids. Extensions to Wertheim's theory have been proposed in the literature, and they are able to capture self-assembly of patchy particles into ordered clusters (88,89). However, a theoretical framework that captures the complexities of protein-protein interactions is absent (84–87). Additionally, the underlying assumptions of these models, such as square-well interactions between bonding sites, is clearly violated due to the induced dipolar interactions that are pervasive in protein association phenomena.

The model just described has been widely used to predict phase behavior of colloidal particle suspensions at their respective pI values or under high salt conditions, where electrostatic interactions are screened (78,79,88–90). We can expect specific (78,79,88–90) and short-ranged interactions in protein solutions to be captured in this highly coarse-grained polymer model, which makes it an excellent choice for estimating $S_o(q)$ in our study; quantitative models for typically short-ranged hydrophobic interactions remain elusive, however (91–94).

The BSS model is a perturbation to the hard sphere interaction potential, wherein a short-range square-well potential precedes the infinitely steep hard-core repulsion, as described below (90,95,96):

$$U_{\mathrm{BSS}}(r) = \begin{cases} \infty\,(r \le \sigma) \\ -u_0(\sigma < r \le \sigma + \Delta)\,, \\ 0(r > \sigma + \Delta) \end{cases} \tag{5}$$

where Δ and u_0 denote the width and depth of the potential well, respectively, and σ denotes the hard core radius. We define a stickiness parameter τ, which describes the strength of interaction between monomers in solution:

$$\tau = \frac{1}{12\varepsilon_p}\exp(u_0/k_{\mathrm{B}}T). \tag{6}$$

The perturbation parameter, $\varepsilon_p = \Delta/(\Delta + \sigma)$ and is fixed at $\varepsilon_p = 0.005$. The BSS model is solved analytically using the Percus-Yevick closure relation to obtain $S_o(q)$ following Pedersen's procedure (97). k_{B} denotes Boltzmann's constant.

The Fourier transform of the perturbation potential, $U'(q)$, consists of a sum of a weak long-range attraction and a long-range repulsion. The weak long-range attraction is modeled using a Yukawa potential (98):

$$U_{AY}(r) = -J\left(\frac{\sigma}{r}\right)\exp[-\kappa_A(r-\sigma)]. \tag{7}$$

The potential well-depth, J, and its range, κ_A, are constrained during fitting to model a weak long-range attraction, while repulsive interactions are modeled using a screened Coulombic potential (1,49,80,91). The attractive component of the long-range potential, $J/k_{\mathrm{B}}T$, is constrained as $10^{-4} \le J/k_{\mathrm{B}}T \le 5$ during fitting to model a weak long-range attraction:

$$U_{SC}(r) = \frac{Z^2e^2}{\varepsilon(1+0.5\kappa\sigma)}\exp\left[\frac{-\kappa(r-\sigma)}{r}\right], \tag{8}$$

where Z is the net charge on the protein, e is elementary charge (1.602×10^{-19} C), ε is the permittivity of the medium, and κ is the inverse Debye screening length, which sets the range of interaction between protein monomers, as follows:

$$\kappa^2 = \frac{8\pi e^2 N_A I}{10^3 \varepsilon k_{\mathrm{B}}T}. \tag{9}$$

Here, N_A and I denote Avogadro's constant and the ionic strength (in units of molar, M) of the solution, respectively. Others have successfully demonstrated that similar approaches are able to capture the dominant intermolecular interactions in globular protein solutions (7,44,49).

RESULTS AND DISCUSSION

We examine the concentration dependence and pH dependence of near-UV CD data, which is an indirect assay for fingerprinting the tertiary structure of proteins (99–101). The path-length dependence of the near-UV CD spectra is eliminated by conversion to molar ellipticity and normalization by concentration. Spectral response in the (260–320) nm wavelength range arises from aromatic amino acids, which have distinct wavelength profiles. For BSA, signals at 262 and 268 nm correspond to optically active transitions of the aromatic residues, such as phenylalanine and tryptophan, and disulfide bonds present in their native state (100,102). Fig. 2, *A–D*, clearly shows that the tertiary structure of BSA molecules changes with pH and concentration in crowded solutions: had the conformation remained unchanged, the spectra for dilute and concentrated solutions would have overlapped.

Although the possibility of surface adsorption on the quartz cuvettes is feasible, it would significantly increase the high tension voltage (absorbance), which was not the case for our measurements; adsorption can therefore be ruled out. It is worth noting that the vertical shift in molar ellipticity cannot be attributed to oligomerization of BSA. Prior studies of the secondary tertiary structure of oligomers demonstrated an absence of changes in the CD spectra as long as the monomer retains its native conformation (100,103). In general, near-UV CD is a low-resolution technique for distinguishing between association states in proteins (104,105). As we do not observe distortion of the peaks or a shift in wavelength of the peak positions, we conclude that aggregation does not influence the CD spectra (100,103). Hence, changes in the molar ellipticity are purely attributed to concentration-dependent conformational changes.

The tertiary structure evidently shows a pH- and concentration dependence, most notably at pH values 3.0 (Fig. 2 *A*), 5.0 (Fig. 2 *B*), and 7.4 (Fig. 2 *D*). To establish a reasonable baseline for our measurements, we include data for urea-denatured BSA at pH values 3.0 and 7.4. These conditions result in complete unfolding of the BSA monomer, where the near-UV CD spectra correspond to that of a random coil. The decrease in molar ellipticity with increasing concentration at 262 and 268 nm and at pH 3.0 indicates that molecular conformation is more compact at higher concentrations, as compared to the expanded conformation at 10 mg/mL (102,106); aromatic residues are buried at high concentrations (30). Conversely, at pH values 5.0 and 7.4, the increase in molar ellipticity at 268 nm arises from aromatic (hydrophobic) residues such as tryptophan and

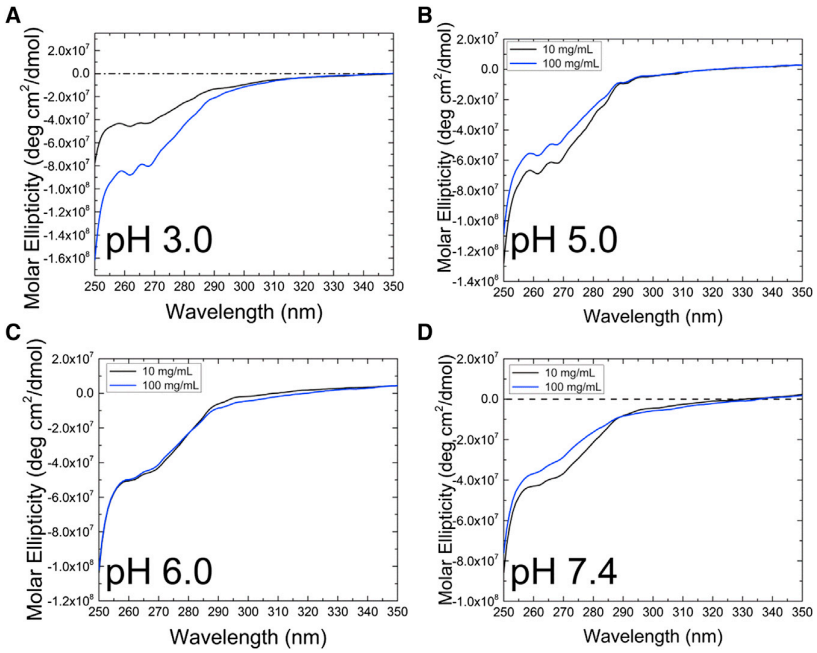

FIGURE 2 Near-UV CD measurements of BSA as a function of c at pH = (*A*) 3.0; (*dash-dot line*) near-UV CD spectra for BSA at pH 3.0 spiked with 8 M urea (*B*) 5.0, (*C*) 6.0, and (*D*) 7.4; (*dashed line*) near-UV CD spectra for BSA at pH 7.4 spiked with 8 M urea. Each dataset is the average of three independent measurements.

phenylalanine, which may promote hydrophobically driven aggregation at high concentrations (83,93,107,108).

Because there are no substantial differences in the spectra for 10 and 100 mg/mL samples at pH 6.0 (Fig. 2 *C*), one infers that conformation is only slightly perturbed as compared to the spectra for pH values 3.0 and 5.0. The conformational changes observed at pH 6.0 are significant, but not as pronounced as pH values 3.0, 5.0, and 7.4. In summary, near-UV CD spectra and their analysis indicates changes in conformation with both pH and concentration, which were most dramatic at pH values 3.0, 5.0, and 7.4. Conformational changes are unsurprising, because proteins are macromolecules rather than rigid ellipsoids or spheres.

In addition to near-UV CD, we also infer conformational changes from intrinsic viscosity measurements (24). We use our intrinsic viscosity measurements to calculate an effective hydrodynamic (viscometric) radius (109),

$$[\eta]M_w = \frac{10\pi N_A}{3}R_H^3, \tag{10}$$

where M_w and R_H denote the BSA molar mass (67 kDa) and hydrodynamic radius, respectively. The reader should note that we are in no way claiming that BSA is a hard sphere under the solution conditions investigated. As shown in Fig. 3, the intrinsic viscosity and effective hydrodynamic radius of BSA are larger at pH values 3.0 and 5.0, compared to pH values 4.0, 6.0, and 7.4. A prior study (25) suggested that BSA undergoes no conformational changes in solutions as concentrated as 40 mg/mL between $4.0 \leq \text{pH} \leq 7.0$. However, we find evidence of conformational changes both at low concentrations via intrinsic viscosity measurements and at higher BSA concentrations from our near-UV CD data. R_H, clearly changes with pH, which is a strong indicator of conformational changes. Complementary evidence of the variations of R_H with pH is also obtained from DLS measurements on dilute BSA solutions, as some of us previously reported (Fig. 4). The R_H is calculated using the Stokes-Einstein relation $R_H = k_B/6\pi\eta D_o$, where D_o is the self-diffusion coefficient. The appreciable change in D_o, and R_H with pH, provides further evidence of conformational changes with pH in dilute solutions. Thus, near-UV CD and intrinsic viscosity measurements reinforce the evidence for conformational changes.

We now turn to measurements of solution structure and thermodynamics via SANS. It should be noted by the reader

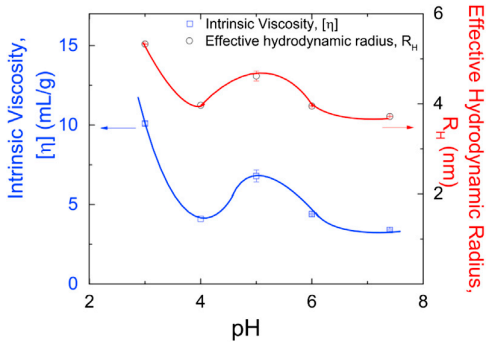

FIGURE 3 Intrinsic viscosity and effective hydrodynamic radius for BSA solutions over a pH and concentration range of $3.0 \leq \text{pH} \leq 7.4$ and $2 \text{ mg/mL} \leq c \leq 12 \text{ mg/mL}$, respectively. In some cases, the uncertainties are smaller than the symbol sizes. Lines are merely guides for the eye.

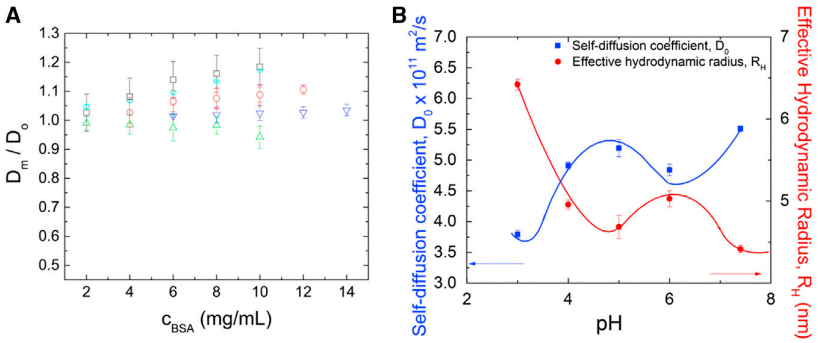

FIGURE 4 (*A*) Mutual diffusion coefficient (D_m) data on BSA solutions normalized by the self-diffusion coefficient (D_o) over a BSA concentration range of 2–12 mg/mL, and pH = 3.0 (*squares*), 4.0 (*circles*), 5.0 (*triangles*), 6.0 (*inverted triangles*), and 7.4 (*diamonds*). (*B*) Self diffusion coefficient and effective hydrodynamic radius, with R_H calculated from the Stokes-Einstein equation.

that both near-UV CD and SANS provide complementary information; however, both techniques can only allow us to determine whether conformational changes occur. The concentration and pH-dependence of the normalized scattered intensity, $I(q)/\phi(1-\phi)$ versus q, is plotted to examine conformational changes with pH and concentration in the high q limit. This normalization procedure accounts for the nonlinear concentration dependence of $I(q)$, because simple $1/c$ normalization is strictly valid in the dilute limit only. Had the chain conformation remained invariant with concentration, $I(q)$ versus q in the high q-range corresponding to scattering from protein monomers $2\ \text{nm}^{-1} \leq q \leq 7\ \text{nm}^{-1}$ would have overlapped. Hence, the high q scattering is entirely due to influence of molecular conformation. Our SANS data for pH values 3.0–7.4 clearly reflect conformational changes. Data in Fig. 5, *A–D*, show that I(high q)/$\phi(1-\phi)$ does not overlap over the investigated range of concentration and pH. The conformational changes that we observe are not an artifact from inappropriate background subtraction, because no clear concentration-dependent incoherent background is apparent. Thus, the changes in the SANS data in the high q limit are attributed to conformational changes.

At pH 3.0, Fig. 5 *A*, *inset*, clearly shows opalescence in BSA solutions up to 200 mg/mL; see picture of vials filled with BSA solution in the inset. Taken together, these data show that prior approaches used in the analysis of small-angle scattering data, which assumed that the form factor is invariant in concentration, are inappropriate for protein solutions where conformation changes with concentration and pH. The reader should note, however, that conformational changes due to specific ion effects cannot be ruled out.

We next turn to modeling of conformational changes based on admittedly colloidal models of the proteins with parameters accounting for conformational effects and with a focus on how changes in conformational structure, identified spectroscopically, impact the strength of the interprotein interactions.

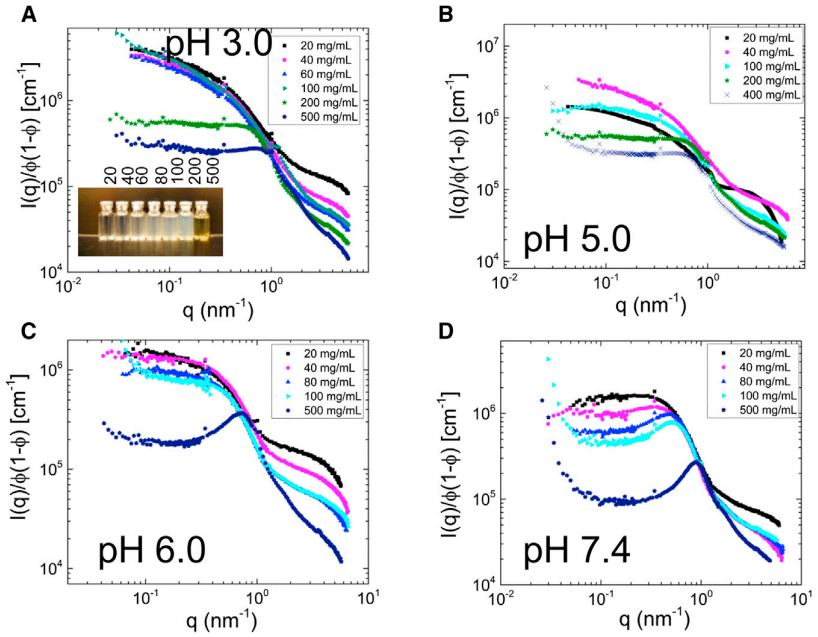

FIGURE 5 Normalized scattered intensity, $I(q)/\phi(1-\phi)$, versus wave-vector q as a function of c at pH = (*A*) 3.0, (*B*) 5.0, (*C*) 6.0, and (*D*) 7.4. (*Inset*) Images of vials filled with BSA solutions at pH 3.0; the number above each vial denotes the BSA concentration in solution in mg/mL.

We attempt to fit our data using simple geometric shapes, such as spheres and ellipsoids to test whether BSA can be described as an effective hard sphere in crowded solutions, as some workers have proposed (110–113). When we attempted to fit our data using an ellipsoid form-factor input into Eq. 3, the calculations simply did not converge. We also used the $P(q)$ for a sphere (Eq. 11, in conjunction with Eq. 3)

$$P(q) = 1/V\left[\frac{3V(\Delta\rho)(\sin(qr) - qr\cos(qr))}{(qr)^3}\right]^2 + B, \quad (11)$$

where V denotes the volume of the sphere. Fig. 6 demonstrates that these fits are poor for high-concentration BSA data across a wide pH range, indicating that BSA in crowded solutions cannot be described as spheres. Because the form factor of an effective hard sphere entity is the same as Eq. 11, we infer that neither a hard sphere nor a so-called effective hard sphere is supported by our scattering data on crowded BSA solutions. BSA neither has an intrinsic viscosity of 2.5, as defined for hydrodynamic hard spheres, nor does it mathematically satisfy the scattering form factor definition of a hard sphere (75,114). Because the hard sphere $P(q)$ does not fit the data, we did not attempt to calculate the intermolecular potential, $U(r)$, or the structure factor, $S(q)$, using the hard-sphere approach.

Having established that simple geometric shapes fail to describe our data, we now wish to use Eq. 3 with the $P(q)$ introduced in Eq. S10 to fit our SANS datasets using the RPA (Eq. 3). We show the results of our fits across the pH and concentration ranges and report the fit parameters in Fig. S2 and Table S3 in the Supporting Material, respectively. At high c for pH values 6.0 and 7.4 in Fig. S2, the RPA model describes the correlation peak in the data at intermediate wave vectors. Although this intermediate-q correlation peak is a ubiquitous feature in charged systems like polyelectrolytes and proteins (7,38,52,115,116), consensus regarding its physical meaning remains elusive. Ise and co-workers (115,116) proposed that the intermediate-q correlation peak seen in globular proteins and polyelectrolytes is related to attractive electrostatic interactions, which lead to the formation of an ordered structure in solution. Their argument would postulate the existence of an intermediate-q peak at pH 3.0, because BSA is highly protonated under acidic conditions; the presence of counterions among charged macroions generates an effective electrostatic attraction that can overcome Coulombic repulsion.

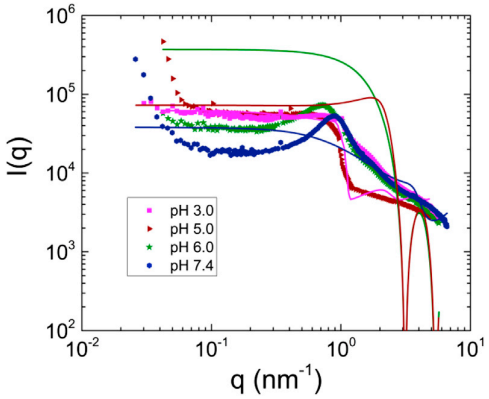

FIGURE 6 Scattered intensity, $I(q)$ versus wavevector q at 400 and 500 mg/mL and pH = (*A*) 3.0, c = 500 mg/mL (*squares*); (*B*) 5.0, c = 400 mg/mL (*triangles*); (*C*) 6.0, c = 500 mg/mL (*stars*); and (*D*) 7.4, c = 500 mg/mL (*pentagons*). (*Solid lines*) Fits from the Supporting Material using a form factor for a sphere (Eq. 11).

Because we find no evidence of a peak under these thermodynamic conditions, attractive electrostatic interactions may not be able to explain the SANS data at pH 3.0. At pH values 6.0 and 7.4, the position of the intermediate-q correlation peak shifts to higher q as concentration increases, suggesting a reduced intermonomer spacing. These trends are qualitatively similar to prior studies of the concentration dependence of intermolecular interactions in unbuffered BSA solutions, and sulfonated poly(styrene) over a wide range of polymer and salt concentration (8,56). The position of the intermediate-q peak showed strong concentration dependence in Zhang et al. (8,56) and was attributed to clusters arising from multipole intermolecular interactions. Liu et al. (7) and Stradner et al. (53) revisited the meaning of the intermediate-q peak in high-concentration lysozyme solutions. They attributed it to intermediate range order, due to the position and lifetime of arrangements associated with this peak. They found that material relaxation rates were essentially unaffected at low concentration and slowed only a few-fold at c ~ 200 mg/mL. They could not find any direct correlation between the presence of an intermediate-q peak and cluster formation. The impact of these transient clusters, if they exist, on solution rheology and the cluster lifetimes, remains to be determined. Indeed, their impact on solution rheology (Fig. 1) is unclear, because the solution viscosity increases at pH values 3.0 and 5.0, while being smaller at pH values 6.0 and 7.4.

Because the protein conformation changes with concentration (Figs. 2, 3, 4, and 5), the balance between attractions and repulsions is altered depending on the extent to which buried hydrophobic or charged residues are exposed (3,14,20,94,107) at various concentrations and pH. Therefore, it is necessary to examine intermolecular interactions that govern the diverse pH- and concentration-dependent thermodynamic properties of BSA solutions. We calculate the effective intermolecular interaction potential, $U(r)$, versus pH using the fit parameters extracted from SANS data: Z, J, κ_A, and τ. In Table S3, we summarize how intermolecular interactions change with concentration and pH. $U(r)$, is the sum of contributions from the Baxter potential, $U_{BSS}(r)$, screened Coulombic potential, $U_{SC}(r)$, and the attractive Yukawa potential, $U_{AY}(r)$. The Baxter potential is

useful for modeling short-range hydrophobic attractions, whereas the Yukawa attraction is necessary for capturing long-range attractions that typify protein solution thermodynamics. Dispersion forces are lumped into the attractive Yukawa term (117,118),

$$U(r) = U_{\mathrm{BSS}}(r) + U_{SC}(r) + U_{AY}(r). \quad (12)$$

We plot $U(r)/k_{\mathrm{B}}T$ for $3.0 \leq \mathrm{pH} \leq 7.4$ in Fig. 7, *A–D*. We deliberately choose not to render r dimensionless using the molecular diameter, σ, because the effective molecular diameter changes with concentration (see Table S3). Some pH-independent trends emerge from these data; we find that the interaction potential shows strong dependence on c and the interaction range reduces with increased concentration. This interaction screening effect, familiar in polymer solutions (91,108,119,120), is accompanied by reduced steepness of repulsion. Thus, at high c, attractive intermolecular attractions influence solution behavior. The delicate balance between short-range attractions and long-range repulsions at high c is one reason why therapeutic protein formulations are often unstable to aggregation (18,20). With the exception of pH 5.0 in Fig. 7 *B*, we find that the c dependence of the interaction potential at pH values 3.0, 6.0, and 7.4 is reminiscent of the theoretical pair potentials for charged colloidal suspensions with added salt.

The steepness and range of repulsion decreases with increasing salt concentration due to a diminished double-layer thickness (91,121,122). The effective net charge, $|Z|$ (Fig. 8), that we extract from fits is consistent with a report by Nossal et al. (29), who performed SANS on BSA solutions up to $c = 200$ mg/mL at pH = 5.9. Our finding that $|Z|$ levels off with increasing c also agrees well with the result of Nossal et al. (29) and the predictions of Israelachvili (91), Leckband and Israelachvili (121), and Verwey and Overbeek (122) of the c dependence of $|Z|$ (Fig. 8), and provides us assurance regarding the soundness and veracity of our results and data analysis. Only indirect estimates of net protein charge can be made at high concentrations. Although assays such as capillary zone electrophoresis (123) and membrane-confined electrophoresis are applied to measure protein net charge, they are limited to dilute ($c < 10$ mg/mL) solutions. Currently, available assays cannot measure net charge directly at high protein concentrations.

There are two obvious physical mechanisms that explain the data in Figs. 7 and 8.

1. Proteins are macroions and contribute to the ionic strength of the solution. They can even have self-buffering capabilities (124,125), which may explain concentration- and pH-dependent intermolecular interaction potential and effective net charge.
2. Because conformation changes with concentration, charged amino-acid residues are buried and condensed with counterions if more compact conformations are adopted. This compaction of protein structure leads to a lower net charge and a reduced interaction range, as seen for polyelectrolytes (126,127).

Short-range attractions dictate solution behavior at the pI of BSA, while Coulombic repulsion dominates at pH distinct from the pI. The results for pH 5.0 in Fig. 7 *B* therefore merit a separate discussion. In this case, we fixed the

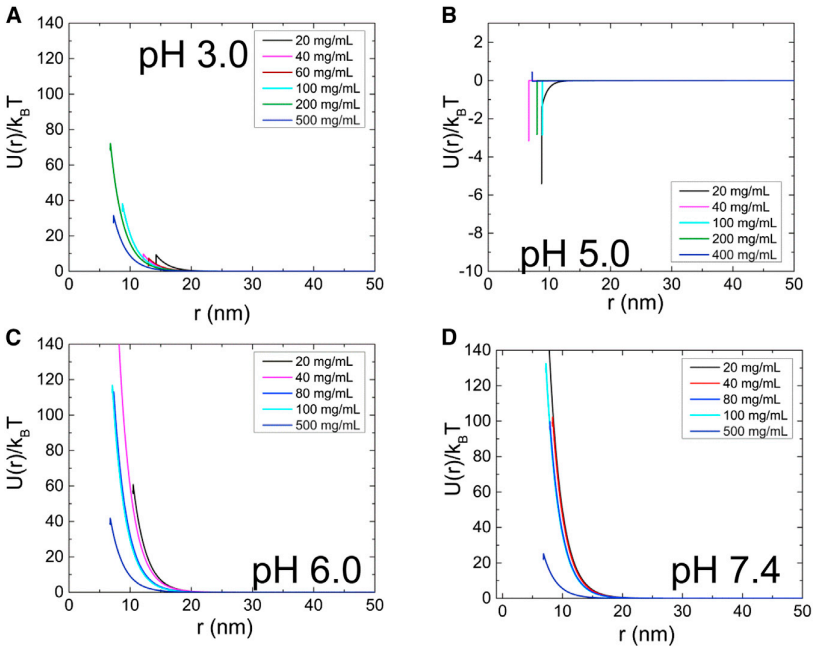

FIGURE 7 Dimensionless intermolecular interaction potential versus radial separation r as a function of c at pH = (*A*) 3.0, (*B*) 5.0, (*C*) 6.0, and (*D*) 7.4.

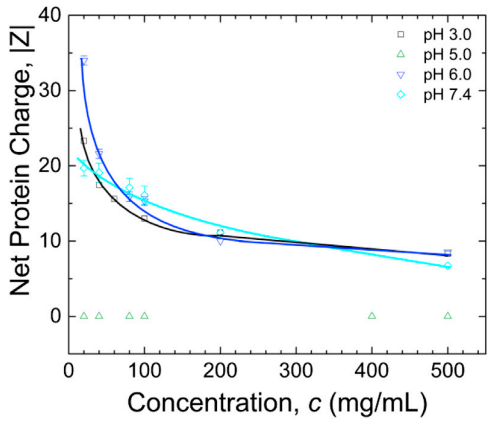

FIGURE 8 Effective net charge versus c for pH = (*A*) 3.0, (*B*) 5.0, (*C*) 6.0, and (*D*) 7.4. Lines that connect points are intended to aid visualization. We force $|Z| = 0$ for pH = 5.0, the pI of BSA.

net charge, $|Z| = 0$ for these fits, because the charge vanishes at the pI. This is a reasonable position in light of our prior study of BSA solution rheology (24) where net attractive interactions dominate at the pI at dilute solution conditions. The data across the entire concentration range reflect net attractive intermolecular interactions. However, there is a nonmonotonic dependence of the range of attraction on c. Variations in the magnitude of the attractive part of the potential due to conformational changes explain Fig. 7 *B*. Orientation-dependent patchy interactions in proteins are captured crudely, at best, in the BSS model. We emphasize that these data invalidate the assumption that the interaction potential of mean force of protein solutions is universally independent of concentration (128,129).

To further explore the diverse pH dependences and concentration dependences of interprotein interactions in BSA solutions, we calculate $S(q)$ (Fig. 9) using the procedure outlined in the Supporting Materials and Methods. For pH values 3.0 and 5.0, a clear minimum in $S(q)$ is observed for $c < 200$ mg/mL at pH 3.0 and $c < 10$ mg/mL at pH 5.0 and over a q-range of 0.01 $nm^{-1} < q < 0.5$ nm^{-1}. Similar behavior observed in BSA solutions at pH 2.0 up to 50 mg/mL (1) and unbuffered BSA solutions at pH 7.0 (9,130) was attributed to net attractive intermolecular interactions.

The observed minimum in $S(q)$ is attributed to the formation of a depletion zone where the local protein density is small. As q tends to 0, spatial correlations of protein monomers become stronger. The value of $S(q \rightarrow 0)$ exceeds that of the primary peak of $S(q)$, which is related to protein clustering (96,131,132), and is a common feature in the structure factors of clustered colloidal dispersions (115,116). We find that the minimum in $S(q)$ is no longer apparent for $c >$ 200 mg/mL at pH 3.0 and is accompanied by a loss of opalescence, which is related to crowding effects that lead to compact conformations in solution (14,107,133) and is not observed at other values of pH. Such changes alter the extent to which hydrophobic and charged residues are exposed in solution.

Indeed, the average size of proteins seems to contract at high protein concentrations, as evidenced by the shift of the peak position of $S(q)$ to higher q. This is a rather familiar phenomenon in synthetic polymers in good solvents, where

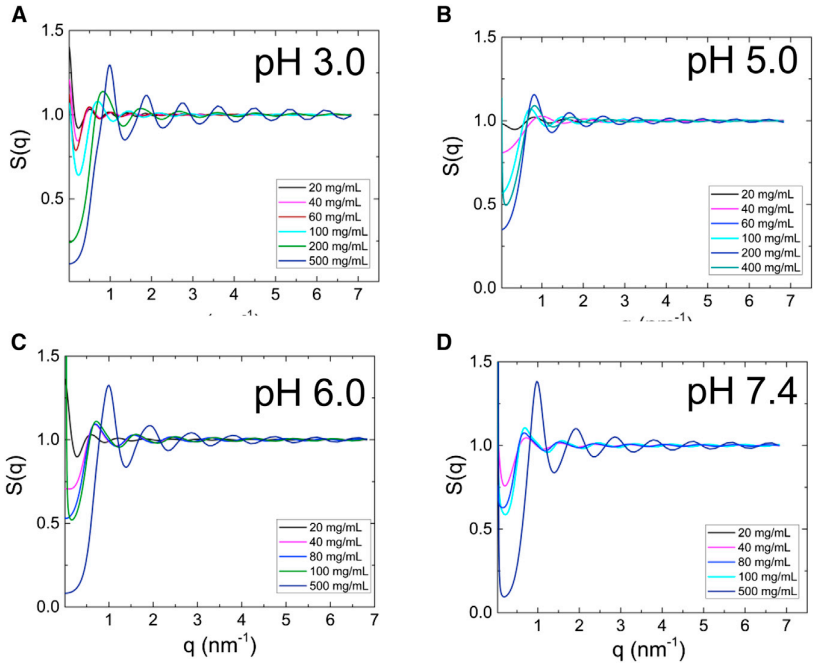

FIGURE 9 Static structure factor $S(q)$ as a function of c at pH = (*A*) 3.0, (*B*) 5.0, (*C*) 6.0, and (*D*) 7.4.

repulsive interparticle interactions at high polymer concentrations cause the polymers to contract. Most published literature on interparticle interactions in protein solutions as well as colloidal suspensions have attributed such shifts of the primary $S(q)$ peak to variations in the net charge or overall protein shape (7,29,38,44,131,132,134). The pH- and concentration-dependence of the primary $S(q)$ peak position also appears to have a strong dependence on c for pH values 3.0 and 5.0 (see Fig. S2). At pH values 6.0 and 7.4, however, the weak concentration dependence of the primary peak indicates that conformational changes are not as pronounced. These data help explain the concentration dependence of viscosity we previously reported, where pH values 3.0 and 5.0 showed a steeper concentration-dependent viscosity (24) as compared to pH values 6.0 and 7.4.

CONCLUSIONS

We have proposed an explanation for the complex pH dependence and concentration dependence of conformation and intermolecular interactions in BSA solutions by considering near-UV CD, intrinsic viscosity, and SANS observations. It is particularly noteworthy that our measurements cover a much wider pH and concentration range than previous studies (1,8,9,23,32,35,46,56,130,135,136). Perhaps unsurprising from a general macromolecular science perspective, our near-UV CD and intrinsic viscosity measurements indicate appreciable changes in BSA conformation (tertiary structure) with protein concentration and pH. The neutron scattering measurements allow us to assess the impact of these changes on the protein intermolecular interactions. The idealized view in the literature that proteins such as BSA are rigid ellipsoidal colloidal particles, whose size and shape are invariant with changes in protein concentration and pH, is found to be untenable. We must then strive to model the conformational changes of proteins upon changes in thermodynamic conditions.

While other workers have literally interpreted BSA neutron scattering measurements in terms of the mathematically expedient colloidal model, we have been cognizant of the limitations of this protein model and have thus adapted these particle-based scattering models to account for molecular size, shape, and interprotein interaction strength effects, which naturally derive from the protein conformational changes evidenced by our independent spectroscopic observations on protein solutions under the same thermodynamic conditions. Although our modeling of the scattering data is admittedly primitive at this stage, basic physical aspects of the protein conformational changes are being quantified, albeit in a highly coarse-grained fashion for reasons of computational tractability in the scattering modeling. We can expect to improve this modeling in the future based on simulation approaches to interpreting our scattering data where the scattering functions are taking from molecular dynamics simulations of the proteins in solution (137). We are also evaluating simulations-based approaches to generate protein conformations and then fitting them to experimental data.

Using a phenomenological form factor with no a priori assumptions of shape and monodispersity, we effectively overcome a limitation of prior studies. The form factor, when combined with our version of the RPA, is able to capture the polydispersity of protein solutions and also the pH-dependent competition between short- and long-range intermolecular interactions. We show that intermolecular interactions and solution structure have a strong pH dependence and concentration dependence. The range of interaction typically decreases with increasing concentration, with the exception of pH = 5.0, which is the isoelectric point of BSA. Variations in the intermolecular interaction potential with concentration and pH as well as conformational changes significantly impact the solution structure and rheology at high protein concentrations. While quantitative measurements of the cluster size distribution and elucidation of the detailed shape of BSA at high concentrations are still necessary but limited by available experimental methods, our data illustrate the nontrivial influence of protein conformational changes at high concentrations.

The thermodynamic and kinetic stability of protein solutions is clearly not solely determined by repulsive electrostatic interactions, but rather by an interplay between short- and long-range attractions and repulsions (13,62,91,121,122,138,139), and their capacity to adjust their shape and thus the nature of the interprotein interactions as thermodynamic conditions. These data reinforce the fact that proteins are macromolecular entities rather than rigid colloidal particles. The range and magnitude of protein-protein interactions and solution structure changes significantly with pH and concentration. We do not imply that aggregation is unimportant for the properties of protein solutions: we are just emphasizing that conformational changes can by themselves strongly influence the viscosity and stability/thermodynamics of protein solutions. The internal degrees of freedom of protein molecules cannot be neglected.

Our findings are not only relevant to deepening the understanding of protein solution thermodynamics and rheology, but assume interdisciplinary significance (1,3,120,127). The effects of pH and concentration on conformation and rheology are highly relevant to developing a more complete picture of the relationship among chain conformation, macromolecular interactions, and the rheology of charged macromolecular solutions. Insights gained from our work should contribute to our understanding of how polyelectrolyte chain conformation relate to anomalous viscosity changes correspondingly observed in synthetic polymers solutions (126,127,140–144).

SUPPORTING MATERIAL

Supporting Materials and Methods (i) Detailed Light Scattering Experimental Methods and Results and (ii) Details of Data Analysis for Small-Angle Neutron Scattering data, three figures, and three tables are available at http://www.biophysj.org/biophysj/supplemental/S0006-3495(14)04765-1.

ACKNOWLEDGMENTS

P.S.S. thanks the MedImmune Postdoctoral Program for fellowship funding. We thank Dr. Steven Bishop (MedImmune), Dr. Flaviu Gruia (MedImmune), Arun Parupudi (MedImmune), Dr. Kalman Migler (National Institute of Standards and Technology (NIST)), and Dr. Debra Audus (NIST) for helpful discussions. We also thank Dr. Vivek Prabhu (NIST), Dr. Charlie Glinka (NIST; retired), and Dr. Ralph Nossal (National Institutes of Health, National Institute of Diabetes and Digestive and Kidney Diseases) for helpful suggestions on a draft of this manuscript. We also thank the three anonymous referees whose thorough reviews and constructive comments have helped improve the quality of this manuscript.

NIST disclaimer: certain commercial equipment, instruments, or suppliers identified in this article specify our procedures adequately. Such identification does not imply recommendation or endorsement by the National Institute of Standards and Technology, nor does it imply that the material or equipment identified are necessarily the best available for the purpose.

SUPPORTING CITATIONS

Reference (145) appears in the Supporting Material.

REFERENCES

1. Barbosa, L. R., M. G. Ortore, …, R. Itri. 2010. The importance of protein-protein interactions on the pH-induced conformational changes of bovine serum albumin: a small-angle x-ray scattering study. *Biophys. J.* 98:147–157.
2. Creighton, T. E. 1993. Proteins: Structures and Molecular Properties. Macmillan, New York.
3. Dill, K. A. 1999. Polymer principles and protein folding. *Protein Sci.* 8:1166–1180.
4. Dobrynin, A. V., R. H. Colby, and M. Rubinstein. 2004. Polyampholytes. *J. Polym. Sci. B Polym. Phys.* 42:3513–3538.
5. Kohn, J. E., I. S. Millett, …, K. W. Plaxco. 2004. Random-coil behavior and the dimensions of chemically unfolded proteins. *Proc. Natl. Acad. Sci. USA.* 101:12491–12496.
6. Jha, A. K., A. Colubri, …, T. R. Sosnick. 2005. Statistical coil model of the unfolded state: resolving the reconciliation problem. *Proc. Natl. Acad. Sci. USA.* 102:13099–13104.
7. Liu, Y., L. Porcar, …, P. Baglioni. 2011. Lysozyme protein solution with an intermediate range order structure. *J. Phys. Chem. B.* 115:7238–7247.
8. Zhang, F., F. Roosen-Runge, …, F. Schreiber. 2012. Hydration and interactions in protein solutions containing concentrated electrolytes studied by small-angle scattering. *Phys. Chem. Chem. Phys.* 14: 2483–2493.
9. Zhang, F., M. W. A. Skoda, …, F. Schreiber. 2007. Protein interactions studied by SAXS: effect of ionic strength and protein concentration for BSA in aqueous solutions. *J. Phys. Chem. B.* 111:251–259.
10. Pathak, J. A., R. R. Sologuren, and R. Narwal. 2013. Do clustering monoclonal antibody solutions really have a concentration dependence of viscosity? *Biophys. J.* 104:913–923.
11. Castellanos, M. M., J. A. Pathak, and R. H. Colby. 2014. Both protein adsorption and aggregation contribute to shear yielding and viscosity increase in protein solutions. *Soft Matter.* 10:122–131.
12. Chi, E. Y., S. Krishnan, …, J. F. Carpenter. 2003. Physical stability of proteins in aqueous solution: mechanism and driving forces in nonnative protein aggregation. *Pharm. Res.* 20:1325–1336.
13. De Young, L. R., A. L. Fink, and K. A. Dill. 1993. Aggregation of globular proteins. *Acc. Chem. Res.* 26:614–620.
14. Dill, K. A. 1985. Theory for the folding and stability of globular proteins. *Biochemistry.* 24:1501–1509.
15. Dill, K. A. 1990. Dominant forces in protein folding. *Biochemistry.* 29:7133–7155.
16. Lilyestrom, W. G., S. Yadav, …, T. M. Scherer. 2013. Monoclonal antibody self-association, cluster formation, and rheology at high concentrations. *J. Phys. Chem. B.* 117:6373–6384.
17. Minton, A. P. 2005. Models for excluded volume interaction between an unfolded protein and rigid macromolecular cosolutes: macromolecular crowding and protein stability revisited. *Biophys. J.* 88:971–985.
18. Shire, S. J., Z. Shahrokh, and J. Liu. 2004. Challenges in the development of high protein concentration formulations. *J. Pharm. Sci.* 93:1390–1402.
19. Cromwell, M. E., E. Hilario, and F. Jacobson. 2006. Protein aggregation and bioprocessing. *AAPS J.* 8:E572–E579.
20. Wang, W., and C. J. Roberts. 2010. Chapter 10: Aggregation and Immunogenicity of Therapeutic Proteins. Wiley Online Library, John Wiley and Sons, New York. http://dx.doi.org/10.1002/9780470769829.ch10.
21. El Kadi, N., N. Taulier, …, M. Waks. 2006. Unfolding and refolding of bovine serum albumin at acid pH: ultrasound and structural studies. *Biophys. J.* 91:3397–3404.
22. Elcock, A. H., and J. A. McCammon. 2001. Calculation of weak protein-protein interactions: the pH dependence of the second virial coefficient. *Biophys. J.* 80:613–625.
23. Li, Y., J. Lee, …, Q. Huang. 2008. Effects of pH on the interactions and conformation of bovine serum albumin: comparison between chemical force microscopy and small-angle neutron scattering. *J. Phys. Chem. B.* 112:3797–3806.
24. Sarangapani, P. S., S. D. Hudson, …, J. A. Pathak. 2013. The limitations of an exclusively colloidal view of protein solution hydrodynamics and rheology. *Biophys. J.* 105:2418–2426.
25. Tanford, C., and J. G. Buzzell. 1956. The viscosity of aqueous solutions of bovine serum albumin between pH 4.3 and 10.5. *J. Phys. Chem.* 60:225–231.
26. Yadav, S., S. J. Shire, and D. S. Kalonia. 2010. Factors affecting the viscosity in high concentration solutions of different monoclonal antibodies. *J. Pharm. Sci.* 99:4812–4829.
27. Yadav, S., S. J. Shire, and D. S. Kalonia. 2011. Viscosity analysis of high concentration bovine serum albumin aqueous solutions. *Pharm. Res.* 28:1973–1983.
28. Zhou, J. X., F. Solamo, …, T. Tressel. 2008. Viral clearance using disposable systems in monoclonal antibody commercial downstream processing. *Biotechnol. Bioeng.* 100:488–496.
29. Nossal, R., C. J. Glinka, and S. H. Chen. 1986. SANS studies of concentrated protein solutions. I. Bovine serum albumin. *Biopolymers.* 25:1157–1175.
30. Tanford, C., J. G. Buzzell, …, S. A. Swanson. 1955. The reversible expansion of bovine serum albumin in acid solutions. *J. Am. Chem. Soc.* 77:6421–6428.
31. Yang, J. T. 1961. The viscosity of macromolecules in relation to molecular conformation. *Adv. Protein Chem.* 16:323–400.
32. Booth, F. 1950. The electroviscous effect for suspensions of solid spherical particles. *Proc. R. Soc. Lond. A Math. Phys. Sci.* 203: 533–551.
33. Liu, H., S. Garde, and S. Kumar. 2005. Direct determination of phase behavior of square-well fluids. *J. Chem. Phys.* 123:174505.

34. Liu, H., S. K. Kumar, and F. Sciortino. 2007. Vapor-liquid coexistence of patchy models: relevance to protein phase behavior. *J. Chem. Phys.* 127:084902–084905.

35. Ikeda, S., and K. Nishinari. 2000. Intermolecular forces in bovine serum albumin solutions exhibiting solidlike mechanical behaviors. *Biomacromolecules.* 1:757–763.

36. Inoue, H., and T. Matsumoto. 1994. Viscoelastic and SAXS studies of the structural transition in concentrated aqueous colloids of ovalbumin and serum albumins. *J. Rheol.* 38:973–988.

37. Kumar, S., V. K. Aswal, and J. Kohlbrecher. 2012. SANS study of lysozyme vs. BSA protein adsorption on silica nanoparticles. *AIP Conf. Proc.* 1447:181–182.

38. Liu, Y., E. Fratini, …, S.-H. Chen. 2005. Effective long-range attraction between protein molecules in solutions studied by small angle neutron scattering. *Phys. Rev. Lett.* 95:118102–118105.

39. Matsumoto, T., and H. Inoue. 1993. Small angle x-ray scattering and viscoelastic studies of the molecular shape and colloidal structure of bovine and rat serum albumins in aqueous systems. *Chem. Phys.* 178:591–598.

40. Mehl, J. W., J. L. Oncley, and R. Simha. 1940. Viscosity and the shape of protein molecules. *Science.* 92:132–133.

41. Neurath, H., G. R. Cooper, and J. O. Erickson. 1941. The shape of protein molecules. II. Viscosity and diffusion studies of native proteins. *J. Biol. Chem.* 138:411–436.

42. Oates, K. M., W. E. Krause, …, R. H. Colby. 2006. Rheopexy of synovial fluid and protein aggregation. *J. R. Soc. Interface.* 3:167–174.

43. Velev, O. D., E. W. Kaler, and A. M. Lenhoff. 1998. Protein interactions in solution characterized by light and neutron scattering: comparison of lysozyme and chymotrypsinogen. *Biophys. J.* 75: 2682–2697.

44. Yearley, E. J., I. E. Zarraga, …, Y. Liu. 2013. Small-angle neutron scattering characterization of monoclonal antibody conformations and interactions at high concentrations. *Biophys. J.* 105:720–731.

45. Sharma, V., A. Jaishankar, …, G. H. McKinley. 2011. Rheology of globular proteins: apparent yield stress, high shear rate viscosity and interfacial viscoelasticity of bovine serum albumin solutions. *Soft Matter.* 7:5150–5160.

46. Edsall, J. T. 1949. The size and shape of protein molecules. *In* Progress in Chemical Research [Fortschritte der Chemischen Forschung], *Vol. 1*.. Springer, Berlin, Germany, pp. 119–174.

47. Lonetti, B., E. Fratini, …, P. Baglioni. 2004. Viscoelastic and small angle neutron scattering studies of concentrated protein solutions. *Phys. Chem. Chem. Phys.* 6:1388–1395.

48. Mertens, H. D., and D. I. Svergun. 2010. Structural characterization of proteins and complexes using small-angle x-ray solution scattering. *J. Struct. Biol.* 172:128–141.

49. Minezaki, Y., N. Niimura, …, T. Katsura. 1996. Small angle neutron scattering from lysozyme solutions in unsaturated and supersaturated states (SANS from lysozyme solutions). *Biophys. Chem.* 58:355–363.

50. Petrescu, A.-J., V. Receveur, …, J. C. Smith. 1997. Small-angle neutron scattering by a strongly denatured protein: analysis using random polymer theory. *Biophys. J.* 72:335–342.

51. Shukla, A., E. Mylonas, …, D. I. Svergun. 2008. Absence of equilibrium cluster phase in concentrated lysozyme solutions. *Proc. Natl. Acad. Sci. USA.* 105:5075–5080.

52. Stradner, A., F. Cardinaux, …, P. Schurtenberger. 2008. Do equilibrium clusters exist in concentrated lysozyme solutions? *Proc. Natl. Acad. Sci. USA.* 105:E75–E76.

53. Stradner, A., H. Sedgwick, …, P. Schurtenberger. 2004. Equilibrium cluster formation in concentrated protein solutions and colloids. *Nature.* 432:492–495.

54. Toft, K. N., B. Vestergaard, …, J. P. Kutter. 2008. High-throughput small angle x-ray scattering from proteins in solution using a microfluidic front-end. *Anal. Chem.* 80:3648–3654.

55. Wu, C. F., and S. H. Chen. 1988. Small angle neutron and x-ray scattering studies of concentrated protein solutions. II. Cytochrome *c*. *Biopolymers.* 27:1065–1083.

56. Zhang, Y., J. F. Douglas, …, E. J. Amis. 2001. Influence of counterion valency on the scattering properties of highly charged polyelectrolyte solutions. *J. Chem. Phys.* 114:3299–3313.

57. Boström, M., F. W. Tavares, …, J. M. Prausnitz. 2006. Effect of salt identity on the phase diagram for a globular protein in aqueous electrolyte solution. *J. Phys. Chem. B.* 110:24757–24760.

58. Lima, E. R., E. C. Biscaia, …, J. M. Prausnitz. 2007. Osmotic second virial coefficients and phase diagrams for aqueous proteins from a much-improved Poisson-Boltzmann equation. *J. Phys. Chem. C.* 111:16055–16059.

59. Tavares, F. W., D. Bratko, …, J. M. Prausnitz. 2004. Ion-specific effects in the colloid-colloid or protein-protein potential of mean force: role of salt-macroion van der Waals interactions. *J. Phys. Chem. B.* 108:9228–9235.

60. Tavares, F. W., and J. M. Prausnitz. 2004. Analytic calculation of phase diagrams for solutions containing colloids or globular proteins. *Colloid Polym. Sci.* 282:620–632.

61. von Solms, N., C. O. Anderson, …, J. M. Prausnitz. 2002. Molecular thermodynamics for fluid-phase equilibria in aqueous two-protein systems. *AIChE J.* 48:1292–1300.

62. Dill, K. A., and S. Bromberg. 2003. Molecular Driving Forces: Statistical Thermodynamics in Chemistry and Biology. Taylor & Francis, New York.

63. Tanford, C. 1961. Physical Chemistry of Macromolecules. Wiley, New York.

64. Harding, S. E., and J. C. Horton. 1992. Analytical Ultracentrifugation in Biochemistry and Polymer Science. Royal Society of Chemistry, Cambridge, UK.

65. Howlett, G. J., A. P. Minton, and G. Rivas. 2006. Analytical ultracentrifugation for the study of protein association and assembly. *Curr. Opin. Chem. Biol.* 10:430–436.

66. Manavalan, P., and W. C. Johnson. 1983. Sensitivity of circular dichroism to protein tertiary structure class. *Nature.* 305:831–832.

67. Pecora, R. 1985. Dynamic Light Scattering: Applications of Photon Correlation Spectroscopy. Springer, New York.

68. Schuck, P. 2003. On the analysis of protein self-association by sedimentation velocity analytical ultracentrifugation. *Anal. Biochem.* 320:104–124.

69. Scott, D. J., S. S. E. Harding, and A. J. Rowe. 2005. Analytical Ultracentrifugation: Techniques and Methods. Royal Society of Chemistry, Cambridge, UK.

70. Some, D., A. Hanlon, and K. Sockolov. 2008. Characterizing protein-protein interactions via static light scattering: reversible heteroassociation. *Am. Biotechnol. Lab.* 26:18–22.

71. Lee, J. J., and D. S. Berns. 1968. Protein aggregation. The effect of deuterium oxide on large protein aggregates of C-phycocyanin. *Biochem. J.* 110:465–470.

72. Arzenšek, D., D. Kuzman, and R. Podgornik. 2012. Colloidal interactions between monoclonal antibodies in aqueous solutions. *J. Colloid Interface Sci.* 384:207–216.

73. Roberts, D., R. Keeling, …, R. Curtis. 2014. The role of electrostatics in protein-protein interactions of a monoclonal antibody. *Mol. Pharm.* 11:2475–2489.

74. Kline, S. R. 2006. Reduction and analysis of SANS and USANS data using IGOR PRO. *J. Appl. Cryst.* 39:895–900.

75. Higgins, J. S., and H. Benoît. 1994. Polymers and Neutron Scattering. Clarendon Press, Oxford, UK.

76. Hansen, J.-P., and I. R. McDonald. 1990. Theory of Simple Liquids. Elsevier, Amsterdam, The Netherlands.

77. Kelkar, V., J. Narayanan, and C. Manohar. 1992. Structure factor for colloidal dispersions. Use of exact potentials in random phase approximation. *Langmuir.* 8:2210–2214.

78. Manohar, C., and V. Kelkar. 1992. Theory of colloidal systems: interactions and structure. *Langmuir.* 8:18–22.

79. Menon, S. V., V. K. Kelkar, and C. Manohar. 1991. Application of Baxter's model to the theory of cloud points of nonionic surfactant solutions. *Phys. Rev. A.* 43:1130–1133.

80. Narayanan, J., and X. Y. Liu. 2003. Protein interactions in undersaturated and supersaturated solutions: a study using light and x-ray scattering. *Biophys. J.* 84:523–532.

81. Wu, J., and J. M. Prausnitz. 1999. Osmotic pressures of aqueous bovine serum albumin solutions at high ionic strength. *Fluid Phase Equilib.* 155:139–154.

82. Svergun, D. I., M. H. Koch, …, R. P. May. 2013. Small Angle X-Ray and Neutron Scattering from Solutions of Biological Macromolecules. Oxford University Press, New York.

83. Lomakin, A., N. Asherie, and G. B. Benedek. 1999. Aeolotopic interactions of globular proteins. *Proc. Natl. Acad. Sci. USA.* 96:9465–9468.

84. Wertheim, M. 1984. Fluids with highly directional attractive forces. I. Statistical thermodynamics. *J. Stat. Phys.* 35:19–34.

85. Wertheim, M. 1984. Fluids with highly directional attractive forces. II. Thermodynamic perturbation theory and integral equations. *J. Stat. Phys.* 35:35–47.

86. Wertheim, M. 1986. Fluids with highly directional attractive forces. III. Multiple attraction sites. *J. Stat. Phys.* 42:459–476.

87. Wertheim, M. 1986. Fluids with highly directional attractive forces. IV. Equilibrium polymerization. *J. Stat. Phys.* 42:477–492.

88. Piazza, R. 2000. Interactions and phase transitions in protein solutions. *Curr. Opin. Colloid Interface Sci.* 5:38–43.

89. Piazza, R., V. Peyre, and V. Degiorgio. 1998. "Sticky hard spheres" model of proteins near crystallization: a test based on the osmotic compressibility of lysozyme solutions. *Phys. Rev. E Stat. Phys. Plasmas Fluids Relat. Interdiscip. Topics.* 58:R2733–R2743.

90. Baxter, R. 1968. Percus-Yevick equation for hard spheres with surface adhesion. *J. Chem. Phys.* 49:2770–2774.

91. Israelachvili, J. N. 2011. Intermolecular and Surface Forces, 3rd Ed. Academic Press, New York.

92. Meyer, E. E., K. J. Rosenberg, and J. Israelachvili. 2006. Recent progress in understanding hydrophobic interactions. *Proc. Natl. Acad. Sci. USA.* 103:15739–15746.

93. Southall, N. T., K. A. Dill, and A. Haymet. 2002. A view of the hydrophobic effect. *J. Phys. Chem. B.* 106:521–533.

94. Baler, K., O. A. Martin, …, I. Szleifer. 2014. Electrostatic unfolding and interactions of albumin driven by pH changes: a molecular dynamics study. *J. Phys. Chem. B.* 118:921–930.

95. De Kruif, C., P. Rouw, …, R. May. 1989. Adhesive hard-sphere colloidal dispersions. A small-angle neutron-scattering study of stickiness and the structure factor. *Langmuir.* 5:422–428.

96. Regnaut, C., and J. Ravey. 1989. Application of the adhesive sphere model to the structure of colloidal suspensions. *J. Chem. Phys.* 91:1211–1221.

97. Pedersen, J. S. 1997. Analysis of small-angle scattering data from colloids and polymer solutions: modeling and least-squares fitting. *Adv. Colloid Interface Sci.* 70:171–210.

98. Mederos, L., and G. Navascues. 1994. Phase diagram of the hard-sphere/attractive Yukawa system. *J. Chem. Phys.* 101:9841–9843.

99. Kelly, S. M., T. J. Jess, and N. C. Price. 2005. How to study proteins by circular dichroism. *Biochim. Biophys. Acta.* 1751:119–139.

100. Woody, R. W. 1995. Circular dichroism. *Methods Enzymol.* 246: 34–71.

101. Yue, K., and K. A. Dill. 1995. Forces of tertiary structural organization in globular proteins. *Proc. Natl. Acad. Sci. USA.* 92:146–150.

102. Price, N. E., N. C. Price, …, J. M. McDonnell. 2005. The key role of protein flexibility in modulating IgE interactions. *J. Biol. Chem.* 280:2324–2330.

103. Hemenger, R. 1978. The effects of band shapes on circular dichroism spectra of chromophore aggregates. *J. Chem. Phys.* 68:1722–1728.

104. Kelly, S. M., and N. C. Price. 2000. The use of circular dichroism in the investigation of protein structure and function. *Curr. Protein Pept. Sci.* 1:349–384.

105. Barrow, C. J., A. Yasuda, …, M. G. Zagorski. 1992. Solution conformations and aggregational properties of synthetic amyloid β-peptides of Alzheimer's disease. Analysis of circular dichroism spectra. *J. Mol. Biol.* 225:1075–1093.

106. Ptitsyn, O. B. 1995. Molten globule and protein folding. *Adv. Protein Chem.* 47:83–229.

107. Dill, K. A. 1990. The meaning of hydrophobicity. *Science.* 250: 297–298.

108. Essafi, W., M.-N. Spiteri, …, F. Boue. 2009. Hydrophobic polyelectrolytes in better polar solvent. Structure and chain conformation as seen by SAXS and SANS. *Macromolecules.* 42:9568–9580.

109. Rubinstein, M., and R. H. Colby. 2003. Polymer Physics. Oxford University Press, Oxford, UK.

110. Minton, A. P., and H. Edelhoch. 1982. Light scattering of bovine serum albumin solutions: extension of the hard particle model to allow for electrostatic repulsion. *Biopolymers.* 21:451–458.

111. Minton, A. P. 2008. Effective hard particle model for the osmotic pressure of highly concentrated binary protein solutions. *Biophys. J.* 94:L57–L59.

112. Minton, A. P. 2007. The effective hard particle model provides a simple, robust, and broadly applicable description of nonideal behavior in concentrated solutions of bovine serum albumin and other nonassociating proteins. *J. Pharm. Sci.* 96:3466–3469.

113. Minton, A. P. 1995. A molecular model for the dependence of the osmotic pressure of bovine serum albumin upon concentration and pH. *Biophys. Chem.* 57:65–70.

114. Roe, R.-J., and R. Roe. 2000. Methods of X-Ray and Neutron Scattering in Polymer Science. Oxford University Press, New York.

115. Ise, N. 1986. Ordering of ionic solutes in dilute solutions through attraction of similarly charged solutes—a change of paradigm in colloid and polymer chemistry. *Angew. Chem. Int. Ed. Engl.* 25:323–334.

116. Ise, N., T. Okubo, …, M. Fujimura. 1983. Ordered structure in dilute solutions of poly-L-lysine as studied by small-angle x-ray scattering. *J. Chem. Phys.* 78:541–545.

117. Castellanos, M. M., J. A. Pathak, …, R. H. Colby. 2014. Explaining the non-Newtonian character of aggregating monoclonal antibody solutions using small-angle neutron scattering. *Biophys. J.* 107: 469–476.

118. Yearley, E. J., P. D. Godfrin, …, Y. Liu. 2014. Observation of small cluster formation in concentrated monoclonal antibody solutions and its implications to solution viscosity. *Biophys. J.* 106:1763–1770.

119. Essafi, W., F. Lafuma, …, C. Williams. 2005. Anomalous counterion condensation in salt-free hydrophobic polyelectrolyte solutions: osmotic pressure measurements. *Europhys. Lett.* 71:938–942.

120. Essafi, W., F. Lafuma, and C. Williams. 1994. Structure of polyelectrolyte solutions at intermediate charge densities. *In* ACS Symposium Series. ACS Publications, Washington, DC, p. 278.

121. Leckband, D., and J. Israelachvili. 2001. Intermolecular forces in biology. *Q. Rev. Biophys.* 34:105–267.

122. Verwey, E. E. J. W., and J. T. G. Overbeek. 1999. Theory of the Stability of Lyophobic Colloids. Dover Publications, Mineola, New York.

123. Gao, J., F. A. Gomez, …, G. M. Whitesides. 1994. Determination of the effective charge of a protein in solution by capillary electrophoresis. *Proc. Natl. Acad. Sci. USA.* 91:12027–12030.

124. Gokarn, Y. R., E. Kras, …, S. Hershenson. 2008. Self-buffering antibody formulations. *J. Pharm. Sci.* 97:3051–3066.

125. Karow, A. R., S. Bahrenburg, and P. Garidel. 2013. Buffer capacity of biologics—from buffer salts to buffering by antibodies. *Biotechnol. Prog.* 29:480–492.

126. Prabhu, V., M. Muthukumar, …, Y. B. Melnichenko. 2003. Polyelectrolyte chain dimensions and concentration fluctuations near phase boundaries. *J. Chem. Phys.* 119:4085–4098.

127. Prabhu, V. M. 2005. Counterion structure and dynamics in polyelectrolyte solutions. *Curr. Opin. Colloid Interface Sci.* 10:2–8.

128. Neergaard, M. S., D. S. Kalonia, …, M. van de Weert. 2013. Viscosity of high concentration protein formulations of monoclonal antibodies of the IgG1 and IgG4 subclass—prediction of viscosity through protein-protein interaction measurements. *Eur. J. Pharm. Sci.* 49: 400–410.

129. Connolly, B. D., C. Petry, …, Y. R. Gokarn. 2012. Weak interactions govern the viscosity of concentrated antibody solutions: high-throughput analysis using the diffusion interaction parameter. *Biophys. J.* 103:69–78.

130. Heinen, M., F. Zanini, …, M. Antalík. 2012. Viscosity and diffusion: crowding and salt effects in protein solutions. *Soft Matter.* 8:1404–1419.

131. Rosenbaum, D., A. Kulkarni, …, C. Zukoski. 1999. Protein interactions and phase behavior: sensitivity to the form of the pair potential. *J. Chem. Phys.* 111:9882–9890.

132. Rosenbaum, D., P. C. Zamora, and C. F. Zukoski. 1996. Phase behavior of small attractive colloidal particles. *Phys. Rev. Lett.* 76:150–153.

133. Zhou, H.-X., G. Rivas, and A. P. Minton. 2008. Macromolecular crowding and confinement: biochemical, biophysical, and potential physiological consequences. *Annu. Rev. Biophys.* 37:375–397.

134. Skibinska, L., J. Gapinski, …, R. Pecora. 1999. Effect of electrostatic interactions on the structure and dynamics of a model polyelectrolyte. II. Intermolecular correlations. *J. Chem. Phys.* 110:1794–1800.

135. Bendedouch, D., S. H. Chen, …, J. S. Lin. 1982. A method for determination of intra- and interparticle structure factors of macroions in solution from small angle neutron scattering. *J. Chem. Phys.* 76:5022–5026.

136. Bloomfield, V. 1966. The structure of bovine serum albumin at low pH. *Biochemistry.* 5:684–689.

137. Clark, N. J., H. Zhang, …, J. E. Curtis. 2013. Small-angle neutron scattering study of a monoclonal antibody using free-energy constraints. *J. Phys. Chem. B.* 117:14029–14038.

138. Carbajal-Tinoco, M., R. Ober, …, C. Williams. 2002. Structural changes and chain conformation of hydrophobic polyelectrolytes. *J. Phys. Chem. B.* 106:12165–12169.

139. Sjöberg, B., and K. Mortensen. 1997. Structure and thermodynamics of nonideal solutions of colloidal particles: investigation of salt-free solutions of human serum albumin by using small-angle neutron scattering and Monte Carlo simulation. *Biophys. Chem.* 65:75–83.

140. Angerman, H. J., and E. Shakhnovich. 1999. Freezing in polyampholytes globules: influence of the long-range nature of the interaction. *J. Chem. Phys.* 111:772–785.

141. Kanai, S., and M. Muthukumar. 2007. Phase separation kinetics of polyelectrolyte solutions. *J. Chem. Phys.* 127:244908.

142. Kantor, Y., and M. Kardar. 1994. Excess charge in polyampholytes. *Europhys. Lett.* 27:643–647.

143. Yamakov, V. V., A. Milchev, …, R. Everaers. 2000. Conformations of random polyampholytes. *Phys. Rev. Lett.* 85:4305–4308.

144. Douglas, J. F., and K. F. Freed. 1994. Competition between hydrodynamic screening ("draining") and excluded volume interactions in an isolated polymer chain. *Macromolecules.* 27:6088–6099.

145. Stafford, 3rd, W. F., and D. A. Yphantis. 1972. Virial expansions for ideal self-associating systems. *Biophys. J.* 12:1359–1365.